Formation of Amorphous $PbCrO_4$ Nanoparticles Depending on the Quantitative Control of Interfacial Water

Chunli Wang,[1, 2] Zhihao, Zhang, [2] Xiaoheng Fu,[1] Jing Zhang, [2] Jan K. G. Dhont [3,4]

[1]*School of Chemistry and Environmental Engineering, China University of Mining and Technology-Beijing, Beijing 100085, China*

[2] *Key Laboratory of Environmental Nano-technology and Health Effect, Research Center for Eco-Environmental Sciences, Chinese Academy of Sciences, Beijing 100085, P. R. China*

[3]*Institute of Biological Information Processing IBI-4, Forschungszentrum Jülich, Leo-Brandt-Str, Jülich D-52425, Germany*

[4]*Department of Physics, Heinrich-Heine-Universität Düsseldorf, Universitätsstrae 1, D-40225 Düsseldorf, Germany*

ABSTRACT. Interfacial water confined in the microemulsions behaviors different to normal bulk water and could affect the reactions involved at the interface. In this work, the content of interfacial and bulk water in the parental microemulsions for the reactions was first quantitatively determined by Fourier-transform infrared (FTIR) spectroscopy. The nucleation and growth of $PbCrO_4$ nanoparticles in the microemulsions were studied, on the basis of the FTIR results. By controlling water ratio in the micellar droplets, amorphous nanoparticles were obtained in the interfacial water, while nanocrystals were produced in the bulk water. The amorphous nanoparticles with defined shapes are quite stable in the microemulsion solution and show no transformation to crystallites for several days. This work offers a delicate way to control the metastable amorphous precursor for follow-up crystallization.

TOC GRAPHICS:

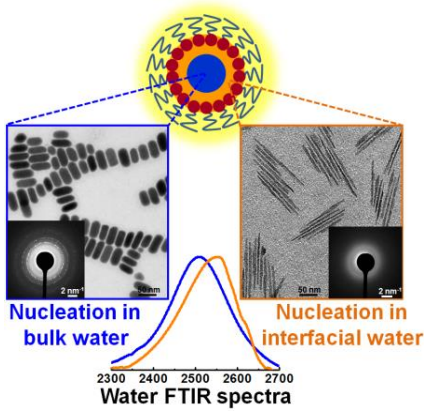

KEYWORDS. Amorphous nanoparticles, Interfacial water, FTIR spectrum, Microemulsion.

Amorphous nanoparticles have recently attracted extensive interest, due to their increasing applications in science and technology.[1] Compared to nanocrystals, amorphous nanoparticles show their special properties, inspired from their long-range disordered structure and higher surface-bulk ratio, in the field of alloy catalysis,[2] magnetism,[3] and corrosion-resistance,[4] surface adsorption of pollutants,[5] and semiconductor photoluminescence.[6]

Amorphous precursors are readily formed prior to their crystalline components,[9] in the light of Ostwald step rules[7,8] that the nucleation and growth in solution often start from the structures that are more similar to the solution. Thereby, the amorphous precursor particles are of considerable importance for understanding the generation and development of nanocrystal structures and properties. For example, amorphous calcium carbonate (ACC) is identified as a postnucleation-stage precursor phase in the formation of calcium carbonate, which determines the produced crystal phases (calcite, vaterite, or aragonite) in biomineralization.[10-12]

According to the classic nucleation theory, the nucleation occurs via either homogeneous nucleation in bulk or heterogeneous nucleation at interfaces. In the latter case, hydration ions are often bound to the organic interfaces or macromolecular matrices, where the interaction between water/ions and interfaces will highly affect the nucleation rates via reducing the interfacial free energy.[13] By virtue of the large interfacial area and ultralow interfacial tension, microemulsions show their priority as the medium to study the effects of water/ion microenvironments on the nucleation and growth of nanoparticles. Compared to free water, water confined in water-in-oil microemulsions shows substantially different dynamic behaviors due to the hydrogen bond interactions with surfactant interfaces. Specifically, the water droplet can be divided into bulk water at the center of the aqueous core, behaving as normal free water, and interfacial water, hydrogen bonded to the hydrophilic headgroup of surfactants. Interfacial water in the

microemulsions shows a distinctively slower relaxation dynamics than bulk water,[14-16] which can give rise to different chemical reactivities in the solvolysis reaction of benzoyl chlorides.[17] Consequently, microemulsions have been employed to produce a wide variety of nanomaterials, including the nanoparticles of gold,[18] mesoporous silica,[19] hydroxyapatite,[20] amorphous calcium carbonate and so on.[21]

However, how the confined water/ions at the interface to easily capture the amorphous precursor phases prior to crystal nucleation, stabilize and extend this metastable state while still in contact with an aqueous phase, and control its dehydration during the transformation to the crystalline state, are still challenges. Lead chromate ($PbCrO_4$), an important solid material that is widely used as a photosensitizer and yellow pigment,[22] shows different UV-visible absorption in amorphous and crystalline phase,[23] but the method of capturing the former under mild conditions has not been reported.

In this work, water-in-oil microemulsions were employed as the reaction medium to study the nucleation and growth of $PbCrO_4$ nanoparticles and their polymorphs developed in solution. By controlling the water content confined in the micellar droplets, amorphous nanoparticles with defined shapes were obtained in the microemulsion solution. The amorphous structures are quite stable and show no transformation in solution for several days. Water-dependent nucleation of nanoparticles was studied by quantifying the content of interfacial and bulk water using liquid FTIR spectroscopy. The interfacial water is viewed to be responsible for the formation of amorphous nanoparticles in the microemulsions.

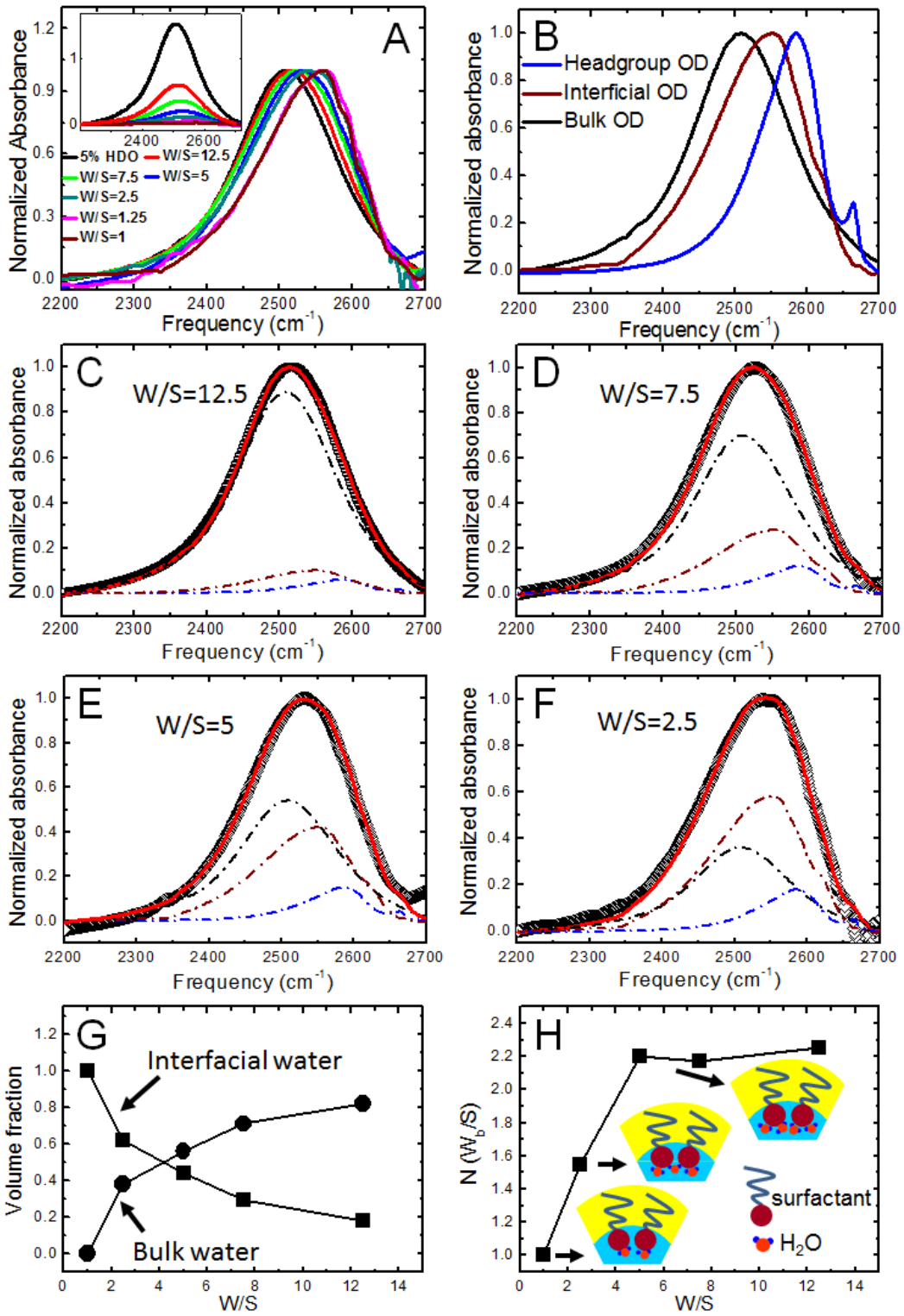

Figure 1. *(A) Normalized FTIR spectra of the OD stretching bands for $C_{12}E_5$ microemulsions of W/S series. The inset shows the spectra of absolute absorbance. (B) Three referee OD bands for*

fitting. (C-F) the fits (solid lines) for the measured spectra (dots) at W/S=12.5 (C), 7.5 (D), 5 (E), and 2.5 (F) by three OD bands (dash-dot lines). (G) The calculated volume fraction of the interfacial water and bulk water versus W/S. (H) The number of the bounded water per surfactant versus W/S. The inserted cartoons represent the interfacial water molecules bounded to the surfactants.

The microstructure of water confined in the parental $C_{12}E_5$ (pentaethyleneglycol monododecylether) microemulsions was first investigated by liquid FTIR spectroscopy, aiming to quantify the content of the interfacial and bulk water. Water solutions used for the measurements were made by adding 2.5% (in weight) of D_2O into H_2O. The purpose of using spectra of isotopically diluted HDO, instead of H_2O, is to simplify the fits and analysis of the FTIR spectra by getting one OD-stretching mode of Gaussian peak (see more details in Experimental Methods and Figure S1 in Supporting Information).[24-26] As shown in Figure 1A, the OD-stretching bands shift to higher frequencies with the decreases of water in the microemulsions, indicating the increased ratio of the interfacial water. Further decreasing water-to-surfactant ratio to *W/S* =1.25 shows no more shift of the absorption peak, overlapping with the spectrum of *W/S* =1. This means that no free water exists in the micellar droplets and all water molecules are hydrogen bonded to the polyoxyethylene headgroups of the surfactants.

In order to determine the ratio of bulk water to interfacial water in the microemulsions, the measured OD stretching spectra (I(ω)) were fitted as the sum of three contributions: bulk water ($I^{bulk}(\omega)$), interfacial water ($I^{interfacial}(\omega)$), and oxyethylene headgroups ($I^{headgroup}(\omega)$) of surfactants due to the isotope exchange. These three referee OD bands are extracted from the measured 5% HDO, the microemulsion at *W/S* =1, and pure deuterated $C_{12}E_5$, respectively (see Figure 1B). By using linear combination of these three referee spectra with a volume fraction Φ,

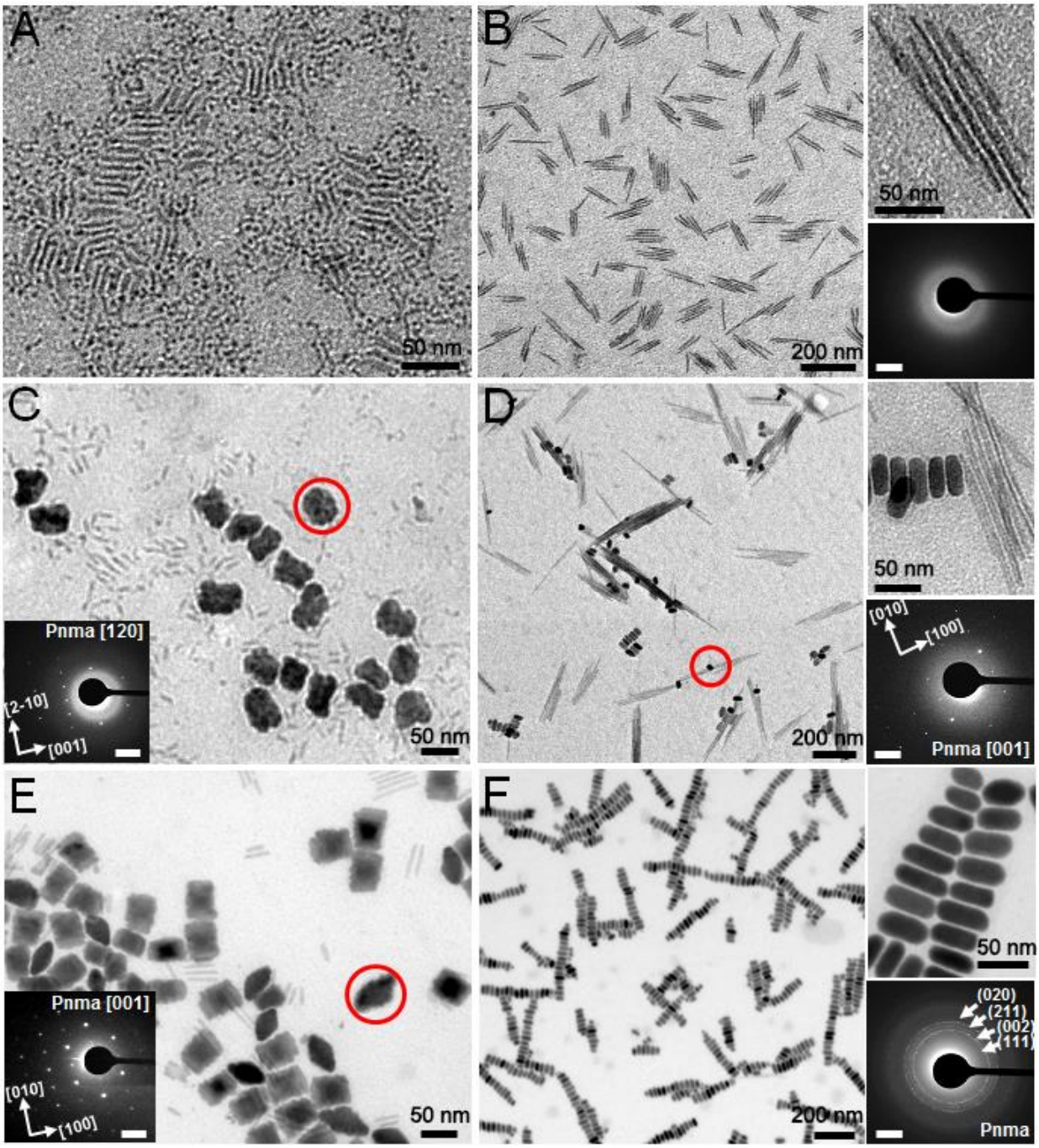

Figure 2. *TEM images of $PbCrO_4$ nanoparticles formed in the microemulsions at W/S=1.25 (A-B), 2.5 (C-D), and 5 (E-F), for 1 min (A, C, E) and 2 h (B, D, F). The upper insets in (B, D, F) show the enlarged images of the produced nanoparticles. The corresponding SAD patterns are shown in the lower insets of (B and F) on the multi-particles, and (C, D, and E) on the marked single-particles, where the space group Pnma and indices of zone axes are presented. Scale bars for all SAD are 2 nm^{-1}.*

$$I(\omega) = \Phi_1 I^{bulk}(\omega) + \Phi_2 I^{interfacial}(\omega) + (1-\Phi_1-\Phi_2) I^{headgroup}(\omega) \quad (1)$$

the OD stretching bands of the microemulsions at different *W/S* ratios were excellently fitted, as shown in Figure 1C-F. From the fits, we can clearly see that at small *W/S* (e.g., *W/S*=2.5), a higher percentage of interfacial water than bulk water exists in the micellar droplets (60% interfacial water vs. 40% bulk water), while more bulk water stays in the droplet as *W/S* increasing, as shown in Figure 1G. The number of interfacial water molecules on every surfactant molecule ($N(W_b/S)$) can be further evaluated by the following equation.

$$N(W_b/S) = ((M_t)(\Phi_2)/(\Phi_2+\Phi_1))/(M_s) \quad (2)$$

Where M_t and M_s respectively represent the total number of molecules of water and surfactant added in the experiment. As seen in Figure 1H, at *W/S*=1 all water is bounded to the surfactants and one water molecule sticks to one surfactant. $N(W_b/S)$ increases to ~1.55 at *W/S* =2.5, and eventually reaches ~2.2 at *W/S*=5, which is followed by a plateau. This means that after *W/S*=5, the interfacial water is saturated and not increased by adding more water. The previous study claimed that 1.5~2 water molecules could directly interact with every oxyethylene group.[27] So it can be deduced that in our microemulsions, the water molecules mainly interact with the surfactants at the interface layer, and the hydrophilic headgroup cannot penetrate into the interior water core. This is in coincidence with the results from the previous work by the water dynamic measurements.[28]

To study the effects of the confined water in the microemulsions on the nucleation and growth of nanoparticles, $PbCrO_4$ nanoparticles formed in the above microemulsions at different W/S ratios were tracked by TEM. The precursor particles at the early stage were captured by taking samples at 1 min. At *W/S*=1.25, the primary nanoparticles are initially small spherical particles, followed by the transformation into elongated particles (Figure 2A). At 2 hours, needle-like nanoparticles of ~200nm in length (*L*) and ~10 nm in width (*D*) are the only final product (Figure

2B), which shows amorphous structure (see the inserted selected area electron diffraction (SAD) pattern in Figure 2B). When the microemulsion of *W/S*=2.5 was employed, two types of prestructures, small elongated particles and big particles with undefined shape, can be seen at 1 min (Figure 2C), which transformed into amorphous needles (*L*~200 nm, *D*~10 nm) and short while thick nanorods (*L*~50 nm, *D*~20 nm), respectively. The SAD patterns reveal that both nanorods and their precursors are orthorhombic crystals (space group: *Pnma*, No. 62), as seen in the insets of Figure 2C and D. Further increasing water ratio to *W/S*=5, more big irregular nanoparticles are formed at the beginning, accompanied with a small amount of elongated particles (Figure 2E). Ubiquitous rod-like crystals are the final products at 2h (Figure 2F). The SAD patterns (the insets in Figure 2E and F) and high resolution TEM images (Figure S2 in Supporting Information) confirm the same crystal structure *Pnma* for both the precursors and the final nanorods.

Combined with the results from FTIR, we can conclude that two different kinds of nucleation modes take place in the bulk and interfacial water. Nanocrystals form in the bulk water, while interfacial water induces amorphous nanoparticles. At *W/S*=1.25, only interfacial water exists in the micellar droplets, resulting in the only product, amorphous needles. Increasing the water content in the microemulsions will bring free water in the core of the droplets, where the nucleation of nanoparticles occurs in the way different to that in the interfacial water (Figure S3) and forms crystallites. Consequently, two kinds of nucleation are simultaneously produced in the microemulsion of *W/S*=5 at the beginning. Although the nucleation in the interfacial water occurs at the early stage, the metastable amorphous precursor phase is readily “consumed” and transformed into the crystallized nanorods, due to the fast inter-droplet exchange kinetics at the

high water content.[29-33] Therefore, nanorod crystallites are observed to be the only final product in solution.

The amorphous nanoparticles formed in the interfacial water can be ascribed to the decreased interfacial free energy of the microemulsions, so that a lower thermodynamic energy barrier to nucleation of the metastable solid phase needs to overcome. Moreover, the structure of metastable phases initially occurring is highly dependent on the hydration environment of ions in solution, on the basis of Ostwald step rules.[7] The hydration ions in interfacial water are strongly hydrogen-bonded to the hydrophilic headgroup of surfactants, where the original hydrogen bonds between the water molecules are destroyed. The fully hydrophilic interfaces give rise to dense but more disordered water structures correlated to the hydrophilic headgroup,[34-36] which results in slow interfacial dynamics that was confirmed by water dynamic measurements.[14] The highly disordering of the interfacial water could suppress the formation of the long distance ordered arrangement of the solid phase during the nucleation. Therefore, the interfacial water of the microemulsion droplets favors to produce amorphous structures.

A typical time series of the nucleation and growth process of the amorphous nanoparticles in the microemulsions at *W/S*=1.25, as imaged by TEM, is shown in Figure 3. Small primary nanoparticles (~5 nm) are first formed just after the initial mixing of the reactants (0 min in Figure 3A). Meanwhile, the primary particles are evidenced to start to grow into elongated particles. At 3 min, more elongated particles of (*L*~50 nm, *D*~5 nm) are obtained (Figure 3B), and these thin ribbon-like particles show a certain flexibility. At 10 min, rigid needle-like nanoparticles (*L*~120 nm, *D*~10 nm) are presented as the main products, accompanied by dissolving of the small primary particles (see Figure 3C). Afterwards, the width of the needles keeps constant at ~10 nm, while the length continuously increases until 2 h and reaches a plateau

at ~220 nm (see Figure 3D-E, and the size evolution with time in Figure 3F). In addition, we count the particle size distribution on histograms during this evolution, indicating the uniformity of the particles around the average size (Figure S4). The needle-like amorphous nanoparticles are quite stable in the microemulsion solution and show no transformation to crystallites for several days (Figure S5 and S6).

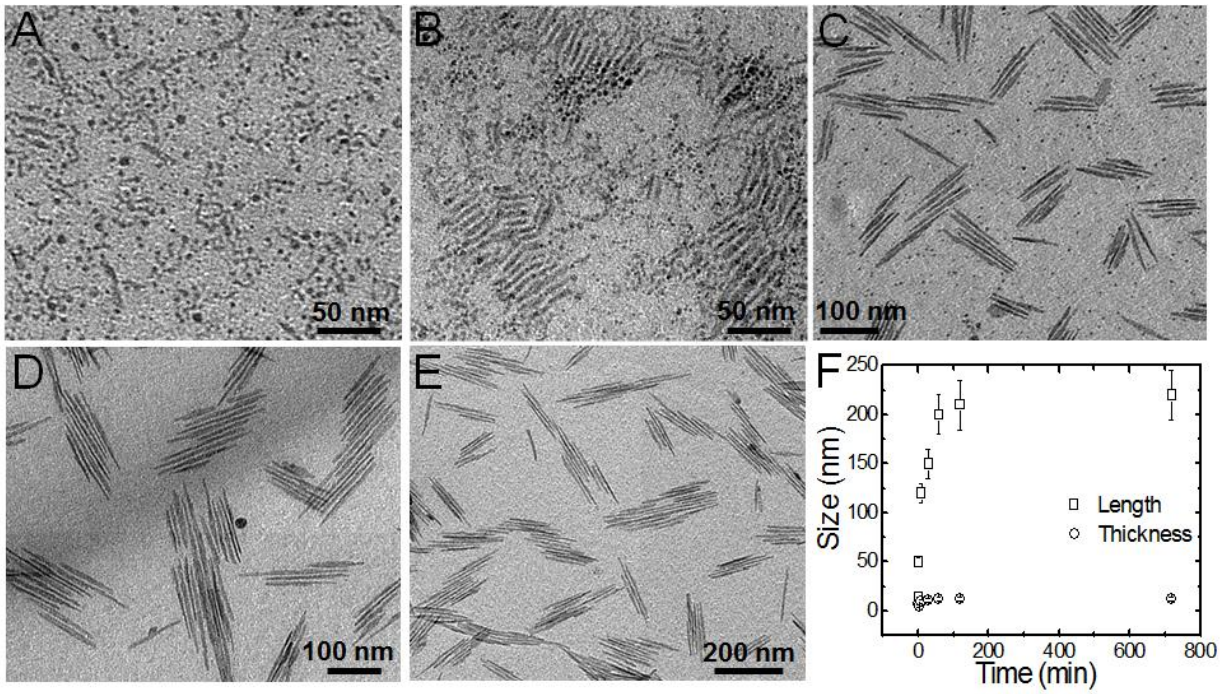

Figure 3. *(A-E) TEM images of amorphous $PbCrO_4$ particles in the microemulsion of W/S=1.25 at different reaction times: 0 min (A), 3 min (B), 10min (C), 1 h (D), and 2 d (E). (F) The size evolution of $PbCrO_4$ needles with time.*

To further investigate the effect of the interfacial water bound to the surfactants on the amorphous nanoparticles, $C_{12}E_4$, having four oxygethylene groups on the hydrophilic part of the surfactants, was employed for making the parental microemulsion. As shown in the FTIR spectrum of Figure 4A, the OD absorption of the $C_{12}E_4$ microemulsion at *W/S*=5 is found to shift a little to the low wavenumbers in comparison with $C_{12}E_5$, which has one more oxygethylene

groups on the hydrophilic part than $C_{12}E_4$ (Figure S7). This means that less water is bound to the $C_{12}E_4$ surfactants, due to less hydrophilic oxygethylene groups. Decreasing the water ratio leads to the OD absorption shifting to a higher frequency, while no more shifting was observed until *W/S*=1. Accordingly, $PbCrO_4$ nanoparticles formed in the $C_{12}E_4$ at small water ratio (*W/S*=1) reveal amorphous structure with a size of ~10 nm in diameter (Figure 4B), while at *W/S*=5 the produced nanoparticles are exclusively crystallites of *Pnma* phase (Figure 4C). From the enlarged image in the inset of Figure 4C, we can see that the ellipsoid-like nanocrystals are ~35 nm in length and ~10 nm in thickness. Compared to the nanoparticles formed in the $C_{12}E_5$ microemulsions, different morphologies of nanoparticles are obtained. However, the interfacial and bulk water confined in the microemulsions shows the same effects on controlling the formation of amorphous and crystalline nanoparticles, respectively.

In summary, the nucleation and growth of $PbCrO_4$ nanoparticles in the nonionic water-in-oil microemulsions have been studied. By controlling the water content in the micellar droplets, amorphous nanoparticles can be obtained at small water ratio, nanocrystals are produced by increasing the water ratio. The interfacial water is responsible for the formation of the amorphous nanoparticles, on the basis of the FTIR analysis on the water confined in the microemulsions. These results enable us to suggest a new field of application of the microemulsions as a competitive alternative to synthesizing new amorphous nanoparticles, stabilizing these metastable phases in aqueous solution, and precisely controlling their transformation into the desired crystalline structures.

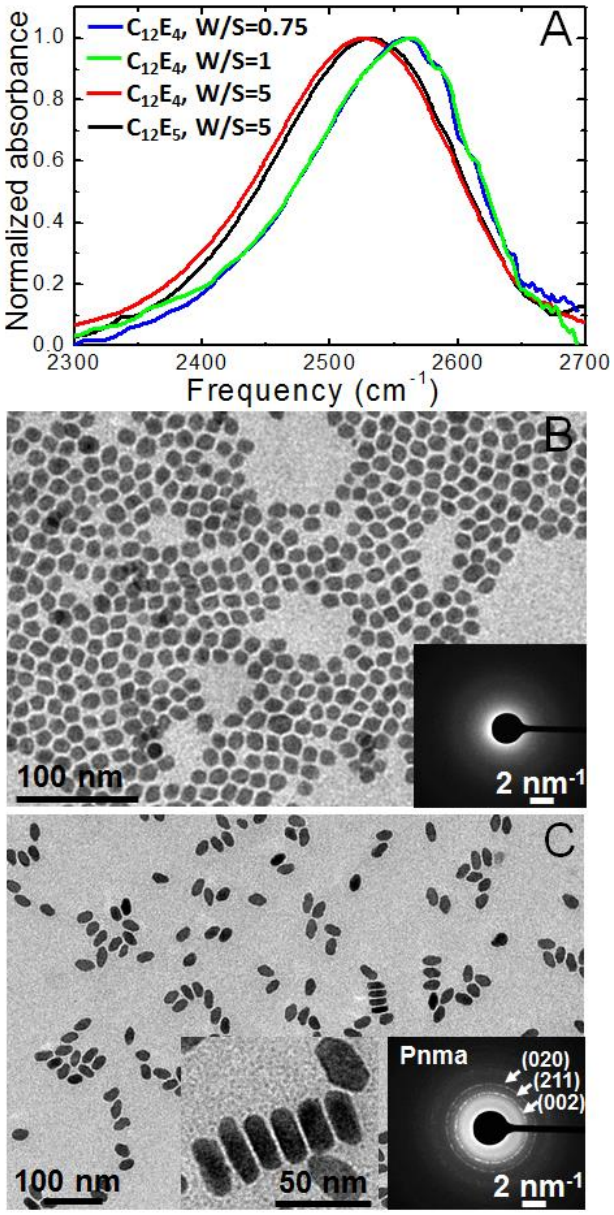

195

196 ***Figure 4.*** *(A) Normalized FTIR spectra of OD stretching bands of $C_{12}E_4$ (W/S=0.75, 1, and 5)*

197 *and $C_{12}E_5$ microemulsions (W/S=5). (B, C) TEM images of $PbCrO_4$ nanoparticles in the $C_{12}E_4$*

198 *microemulsions at W/S=1.25 (B) and W/S=5 (C) for 2h. The inset of (B) is the corresponding*

199 *SAD pattern, and the insets of (C) are the enlarged image (left) and SAD pattern (right).*

200

201 ASSOCIATED CONTENT

Supporting Information.

Detailed experimental methods, FTIR spectra and the fits for H_2O and 5% HDO in H_2O, and HRTEM images for $PbCrO_4$ nanocrystals.

AUTHOR INFORMATION

Corresponding Author

*Email: jingzhang@rcees.ac.cn

Notes

The authors declare no competing financial interests.

ACKNOWLEDGMENT

The authors acknowledge the financial support from the National Key Research and Development Program of China (2017YFA0207204 and 2016YFA0203101), the National Natural Science Foundation of China (21876190 and 21836002), the Fundamental Research Funds for the Central Universities (2020001840), and the Key Research and Development Program of Ningxia (2017BY064).

REFERENCES

(1) Hoang, V. V.; Ganguli, D.. Amorphous Nanoparticles — Experiments and Computer Simulations. *Phys. Rep.* **2012**, *518*, 81–140.

(2) Suslick, K. S.; Choe, S. B.; Cichowlas, A. A.; Grinstaff, M. W. Sonochemical Synthesis of Amorphous Iron. *Nature* **1991**, *353*, 414–416.

(3) Zboril, R.; Machala, L.; Mashlan, M.; Tucek, J.; Muller, R.; Schneeweiss, O. Magnetism of Amorphous Fe_2O_3 Nanopowders Synthesized by Solid-State Reactions. *Phys. Status Solidi C* **2004**, *1*, 3710–3716.

(4) Hashimoto, K.; Park, P. Y.; Kim, J. H.; Yoshioka, H.; Mitsui, H.; Akiyama, E.; Habazakia, H.; Kawashimaa, A.; Asamia, K.; Grzesikb, Z.; Mrowecb S. Recent Progress in Corrosion-Resistant Metastable Alloys. *Mat. Sci. Eng. A* **1995**, *198*, 1–10.

(5) Basnet, P.; Zhao, Y. Superior Dye Adsorption Capacity of Amorphous WO_3 Sub-Micrometer Rods Fabricated by Glancing Angle Deposition. *J. Mater. Chem. A* **2014**, *2*, 911–914.

(6) Chini, T. K.; Datta, D. P.; Facsko, S.; Mücklich, A. Room Temperature Photoluminescence from the Amorphous Si Structure Generated under keV Ar-Ioninduced Surface Rippling Condition. *Appl. Phys. Lett.* **2008**, *92*, 101919–101921.

(7) Ostwald, W. Studien uber die Bildung und Umwandlung fester Korper. *Z. Phys. Chem.* **1897**, *22*, 289–330.

(8) Navrotsky, A. Energetic Clues to Pathways to Biomineralization: Precursors, Clusters, and Nanoparticles. *Proc. Natl. Acad. Sci. U.S.A.* **2004**, *101*, 12096–12101.

(9) Baumgartner, J.; Dey, A.; Bomans, P. H. H.; Le Coadou, C.; Fratzl, P.; Sommerdijk, N. A. J. M.; Faivre, D. Nucleation and Growth of Magnetite from Solution. *Nature Mater.* **2013**, *12*, 310–314.

(10) Gebauer, D.; Völkel, A.; Cölfen, H. Stable Prenucleation Calcium Carbonate Clusters. *Science* **2008**, *322*, 1819–1822.

(11) Faatz, M.; Gröhn, F.; Wegner, G. Amorphous Calcium Carbonate: Synthesis and Potential Intermediate in Biomineralization. *Adv. Mater.* **2004**, *16*, 996–1000.

(12) Gal, A.; Habraken, W.; Gur, D.; Fratzl, P.; Weiner, S.; Addadi, L. Calcite Crystal Growth by a Solid-State Transformation of Stabilized Amorphous Calcium Carbonate Nanospheres in a Hydrogel. *Angew. Chem. Int. Ed.* **2013**, *52*, 4867–4870.

(13) Hu, Q.; Nielsen, M. H.; Freeman, C. L.; Hamm, L. M.; Tao, J.; Lee, J. R. I.; Han, T. Y. J.; Becker, U.; Harding, J. H.; Dove, P. M.; De Yoreo, J. J. The Thermodynamics of Calcite Nucleation at Organic Interfaces: Classical vs. Non-Classical Pathways. *Faraday Discuss.* **2012**, *159*, 509–523.

(14) Moilanen, D. E.; Levinger, N. E.; Spry, D. B.; Fayer, M. D. Confinement or the Nature of the Interface? Dynamics of Nanoscopic Water. *J. Am. Chem. Soc.* **2007**, *129*, 14311–14318.

(15) Levinger, N. E.; Swafford, L. A. Ultrafast Dynamics in Reverse Micelles. *Annu. Rev. Phys. Chem.* **2009**, *60*, 385–406.

(16) Fayer, M. D. Dynamics of Water Interacting with Interfaces, Molecules, and Ions. *Acc. Chem. Res.* **2012**, *45*, 3–14.

(17) García-Rio, L.; Leis, J. R.; Moreira, J. A. Reactivity in Water/Oil Microemulsions. Influence of Sodium Bis(2-ethylhexyl)sulfosuccinate/Isooctane/Water Microemulsions on the Solvolysis Mechanism of Substituted Benzoyl Chlorides. *J. Am. Chem. Soc.* **2000,** *122,* 10325–10334.

(18) Rajapantulu, A.; Bandyopadhyaya, R. Formation of Gold Nanoparticles in Water-in-Oil Microemulsions: Experiment, Mechanism, and Simulation. *Langmuir* **2021**, 37, 6623-6631.

(19) Ren, D.; Xu, J.; Chen, N.; Ye, Z.; Li, X.; Chen, Q.; Ma, S. Controlled synthesis of mesoporous silica nanoparticles with tunable architectures via oil-water microemulsion assembly process. *Colloids Surf. A Physicochem. Eng. Asp.* **2021**, 611, 125773.

(20) Collins Arun Prakash, V.; Venda, I.; Thamizharasi, V. Synthesis and characterization of surfactant assisted hydroxyapatite powder using microemulsion method. *Mater. Today* **2021**, 49, 3165-3168.

(21) Stawski, T. M.; Roncal-Herrero, T.; Fernandez-Martinez, A.; Matamoros-Veloza, A.; Kröger, R.; Benning, L. G., "On demand" triggered crystallization of $CaCO_3$ from solute precursor species stabilized by the water-in-oil microemulsion. *Phys. Chem. Chem. Phys.* **2018**, 20, 13825-13835.

(22) Liang, J.; Li, Y., Synthesis and characterization of lead chromate uniform nanorods. *J. Cryst. Growth* **2004**, 261, 577-580.

(23) Mao, C.-J.; Wu, X.-C.; Zhu, J.-J., Shape-controlled synthesis of $PbCrO_4$ micro/nanostructures and their luminescent properties. J. Nanosci. Nanotechnol. **2010**, 10, 4906-4913.

(24) Waldron, R. D. Infrared Spectra of HDO in Water and Ionic solutions. *J. Chem. Phys.* **1957**, *26*, 809–814.

(25) Hornig, D. F. On the Spectrum and Structure of Water and Ionic Solutions. *J. Chem. Phys*. **1964,** *40*, 3119–3120.

(26) Falk, M.; Ford, T. A. Infrared Spectrum and Structure of Liquid Water. *Can. J. Chem*. **1966**, *44*, 1699–1707.

285 (27) Micali, N.; Vasi, C.; Mallamace, F.; Corti, M.; Degiorgio, V. Raman Scattering and Water
286 Structure in Nonionic Amphiphile Solutions. *Phys*. *Rev*. *E* **1993**, *48*, 3661–3666.

287 (28) van der Loop, T.H.; Panman, M. R.; Lotze, S.; Zhang, J.; Vad, T.; Bakker, H. J.; Sager,
288 W.; Woutersen S. Structure and Dynamics of Water in Nonionic Reverse Micelles: A Combined
289 Time-Resolved Infrared and Small Angle X-Ray Scattering Study. *J. Chem. Phys.* **2012**, *137*,
290 044503.

291 (29) Fletcher, P. D. I.; Howe, A. M.; Robinson, B. H. The Kinetics of Solubilisate Exchange
292 between Water Droplets of a Water-in-Oil Microemulsion. *J. Chem. Soc., Faraday Trans.1* **1987**,
293 *83*, 985–1006.

294 (30) Bagwe, R. P.; Khilar, K. C. Effects of Intermicellar Exchange Rate on the Formation of
295 Silver Nanoparticles in Reverse Microemulsions of AOT. *Langmuir* **2000**, *16*, 905–910.

296 (31) Kitchens, C. L.; Chandler McLeod M.; Roberts, C. B. Solvent Effects on the Growth and
297 Steric Stabilization of Copper Metallic Nanoparticles in AOT Reverse Micelle Systems. *J. Phys.*
298 *Chem. B* **2003**, *107*, 11331–11338.

299 (32) Ganguli, A. K.; Ganguly, A.; Vaidya, S. Microemulsion-Based Synthesis of
300 Nanocrystalline Materials. *Chem. Soc. Rev.* **2010**, *39*, 474–485.

301 (33) Zhang, J.; Lang, P. R.; Pyckhout-Hintzen, W.; Dhont, J. K. G. Controllable Synthesis and
302 Self-Assembly of $PbCO_3$ Nanorods in Shape-Dependent Nonionic w/o Microemulsions. *Soft*
303 *Matter* **2013**, *9*, 7576–7582.

304 (34) Limmer D. T.; Chandler, D. Phase Diagram of Supercooled Water Confined to
305 Hydrophilic Nanopores. *J. Chem. Phys.* **2012**, *137*, 044509.

(35) Rasaiah, J. C.; Garde, S.; Hummer, G. Water in Nonpolar Confinement: From Nanotubes to Proteins and Beyond. *Annu. Rev. Phys. Chem.* **2008**, *59*, 713–740.

(36) Medders G. R.; Paesani, F. Water Dynamics in Metal−Organic Frameworks: Effects of Heterogeneous Confinement Predicted by Computational Spectroscopy. *J. Phys. Chem. Lett.* **2014**, *5*, 2897−2902.